Published in final edited form as:
Opt Express. 2012 March 26; 20(7): 7564–7574.

Automated measurement of choroidal thickness in the human eye by polarization sensitive optical coherence tomography

Teresa Torzicky, **Michael Pircher**, **Stefan Zotter**, **Marco Bonesi**, **Erich Götzinger**, and **Christoph K. Hitzenberger***
Center for Medical Physics and Biomedical Engineering, Medical University of Vienna, A-1090 Vienna, Austria

Abstract

We present a new method to automatically segment the thickness of the choroid in the human eye by polarization sensitive optical coherence tomography (PS-OCT). A swept source PS-OCT instrument operating at a center wavelength of 1040 nm is used. The segmentation method is based entirely on intrinsic, tissue specific polarization contrast mechanisms. In a first step, the anterior boundary of the choroid, the retinal pigment epithelium, is segmented based on depolarization. In a second step, the choroid-sclera interface is found by using the birefringence of the sclera. The method is demonstrated in five healthy eyes. The mean repeatability (standard deviation) of thickness measurement was found to be 18.3 μm.

1. Introduction

Optical coherence tomography (OCT) was introduced two decades ago [1] as a non-invasive modality for imaging transparent and translucent samples and tissues with resolution of a few μm [2, 3]. The first (and still dominating) application field of OCT was ophthalmology, where OCT revolutionized retinal imaging and diagnostics [4, 5]. The introduction of the spectral domain (SD) principle [6–8] caused a paradigm shift in OCT technology. Its improved sensitivity [9–11] enables modern commercial OCT scanners to operate at imaging speeds beyond 20 kA-lines/s. They operate in the 800 nm wavelength regime and achieve an axial resolution on the order of 5 μm, providing high-quality images of the retina, from the inner limiting membrane down to the retinal pigment epithelium (RPE). However, presently available commercial OCT systems still have two shortcomings: (i) Imaging of deeper layers, beyond the RPE, is hindered by scattering and absorption of the sampling light in the RPE. (ii) They acquire images just based on backscattered intensity which does not provide a tissue specific contrast.

It has been shown that the use of longer wavelengths can overcome the first problem. The optimum wavelength regime for OCT imaging beyond the RPE is around 1050 nm where

*christoph.hitzenberger@meduniwien.ac.at.

OCIS codes: (170.4500) Optical coherence tomography; (230.5440) Polarization-selective devices; (170.4470) Ophthalmology; (170.4580) Optical diagnostics for medicine.

Europe PMC Funders Author Manuscripts

scattering and absorption of the RPE are reduced and water absorption has a local minimum [12–15]. The use of this wavelength enabled imaging of the choroid down to the choroid-sclera interface (CSI). The introduction of this method allowed to measure the thickness of the choroid, a quantity of great interest for the study of ocular disorders like high myopia, diabetic retinopathy, central serous chorioretinopathy, etc. Recent studies demonstrate the interest to measure the choroidal thickness by this technique (cf., e.g., [16–18]). However, in most of these studies, the CSI is segmented manually, which is problematic since it is time consuming and largely subjective. Only very recently, a first study employing an automated segmentation algorithm based on a statistical model and texture analysis was reported [19]. This study used exclusively intensity based data.

Polarization sensitive (PS) OCT [20, 21] is a functional extension of OCT that takes advantage of the additional information carried in the light's polarization state. Thereby, PS-OCT can be used to solve the second problem mentioned above. Several structures in the ocular fundus can change the polarization state of the sampling beam: there are birefringent structures like the retinal nerve fiber layer [22, 23], Henle's fiber layer [24, 25], the sclera [26, 27], or scar tissue [28]. These structures introduce a phase retardation between beam components of orthogonal polarization state which can be used for contrasting or to perform quantitative measurements [29–32]. The RPE and other pigmented tissues like choroidal melanoma or naevi act as depolarizers, i.e. scramble the polarization state of backscattered light [25, 33, 34]. This effect can be used to segment the RPE and associated lesions by its intrinsic, tissue specific polarization contrast [35–37].

In this paper, we use PS-OCT at 1040 nm, to the best of our knowledge for the first time, to automatically segment the thickness of the choroid by an algorithm that exploits two tissue polarization properties: in a first step, the RPE is segmented based on its depolarizing effect; in a second step, the CSI is segmented based on the birefringence of the sclera. Finally, the difference between the two layers is calculated. We demonstrate the method in five healthy volunteers, present repeatability data, and discuss the results in relation to intensity based manual measurements.

2. Methods

2.1 Instrument

We used a PS-OCT setup based on principles reported previously [38]. The main changes made were as follows: (i) The super luminescent diode (SLD; center wavelength 840 nm) was replaced by a swept source (Axsun Inc.) operating at a center wavelength of 1040 nm at a scanning speed of 100 kHz. The sweep range is 110 nm, providing an axial resolution of 7.9 μm in air or 5.6 μm in tissue (assuming a refractive index of 1.4). (ii) The bulk optic Michelson interferometer was replaced by a bulk optic Mach Zehnder interferometer. (iii) The spectrometer based detection unit was replaced by a dual balanced detection scheme employing InGaAs detectors with a cutoff frequency of 350 MHz (Thorlabs Inc.) and a 2-channel 12 bit AD board operating at 500 MSamples/s (Alazartech). The eye was illuminated by a power of 2 mW providing a sensitivity of ~102 dB and a roll off of ~4 dB over 3 mm optical imaging depth.

The principles of polarization sensitive detection were similar as in our previous work [38, 39]: the sample (eye) was illuminated by circularly polarized light, and a polarization sensitive detection was performed in two orthogonal polarization channels simultaneously. This allowed the simultaneous measurement of the following parameters: reflectivity, retardation, optic axis orientation, and degree of polarization uniformity (DOPU) [35].

2.2 Imaging protocol

In this work, B-scan series of the human retina were recorded centrally through the fovea. A B-scan series consisted of 50 B-scans (1000 A-scans each, scan angle ~20°) recorded at the same position within 0.5 s. B-scans were averaged (see below) to reduce speckle noise and improve image quality. To determine the repeatability of our results, each subject was imaged five times. The subjects sat back and were re-aligned between the measurements.

Five healthy human subjects were enrolled in the study. Their age ranged from 25 to 54 years, refraction ranged from 0 to −3.5 diopters. Since the iris color of the subjects varied considerably (blue, grey, green, brown), a statistically significant correlation of iris color and choroid pigmentation/penetration was not possible within this small study group. The subjects were imaged after the nature and possible consequences of the study were explained and full informed consent was obtained. The study was approved by the ethics committee of the Medical University of Vienna and adhered to the tenets of the Declaration of Helsinki.

2.3 Data processing

After standard Fourier domain OCT data preprocessing (fixed pattern noise removal, rescaling of the spectral data to remove sweep nonlinearities, spectral side lobe suppression by a Hanning window, zero padding, dispersion compensation) an inverse FFT is performed. From the resulting complex data set, amplitude and phase information is derived for each polarization channel. From these quantities, the reflectivity, retardation, and optic axis orientation can be calculated as described previously [38, 39].

In a next step, residual motion artifacts between the B-scans of a series were corrected by cross-correlating the B-scans (Image J, MultiStackReg). Afterwards, B-scans were averaged to reduce speckle noise and to improve image quality. The following data sets were generated in this way (details of the used averaging procedures can be found in ref [40].): intensity (average of reflectivity images), retardation (calculating retardation first for each frame, then averaging the retardation frames), and DOPU (temporal DOPU window, i.e., Stokes vector elements averaged pixel wise over successive B-scans).

In the following step, the RPE and the CSI were segmented based on their polarization properties. The individual segmentation procedures are described with reference to Fig. 1 which shows an example of averaged images derived from a B-scan series. The intensity image (Fig. 1(a)) shows a cross section where all the major retinal layers can be seen. The choroid can be clearly identified, demonstrating the improved imaging depth of the 1040 nm SS PS-OCT system. Behind the area showing large blood vessels (dark patches surrounded by brighter structures, perhaps vessel walls), an area of rather uniform backscattered intensity that decreases with depth can be observed.

We start by segmenting the RPE which can be regarded as the anterior boundary of the choroid (in healthy eyes, the RPE is indistinguishable from Bruch's membrane). In the intensity image, the RPE is observed as the last bright boundary at the posterior side of the retina. Its intensity is approximately similar to that of the two boundaries located immediately anterior to the RPE, the end tips of the photoreceptors (ETPR, the layer immediately adjacent to the RPE), and the boundary between inner and outer photoreceptor segments (IS/OS, the layer anterior to the ETPR). However, the RPE shows a very different contrast behavior in polarization sensitive images. As can be seen in the DOPU image (Fig. 1(b)), the RPE strongly depolarizes backscattered light (greenish band). This intrinsic, tissue specific contrast can be used to directly segment the RPE. We extract the RPE by applying a thresholding algorithm that segments pixels below a DOPU threshold of $DOPU_{thr} < 0.8$. We then fit a polynomial of 4th order to the segmented pixels. The result is a line that marks the position of the RPE. Figure 1(e) shows an intensity image with the segmented RPE line shown in red. This line is taken as the anterior boundary of the choroid.

Figure 1(c) shows the retardation image. The rather constant blue color observed in the layers anterior to the RPE indicates that these layers essentially preserve the polarization state of the incident beam. The RPE is observed as a cyan-green band; this color is caused by averaging the randomly distributed polarization states generated by the depolarizing RPE over the 50 successive frames. Beneath the RPE, the choroid shows again blue color, indicating polarization preservation. The patches of somewhat lighter blue and cyan indicate slight depolarization by choroidal pigments and are also partly caused by noise due to low signal intensity; this can be observed especially in the areas corresponding to vessels (dark patches in the intensity image). Further below, a color change to cyan, green, and yellow can be observed. This indicates phase retardation caused by the birefringent sclera. Deeper areas of the sclera are shown in grey. This indicates that the signal obtained from the corresponding area is not reliable enough to calculate correct retardation values. Two conditions can lead to this gating out of signals: (i) the intensity is too low, which distorts measured retardation [41]; this is checked by applying an intensity threshold (areas of signal-to-noise ratio below 7 dB in the averaged B-scans are excluded). (ii) The signal originates from multiple scattering which causes a random polarization state. This is checked by applying a DOPU threshold (signals with $DOPU < 0.3$ are excluded).

We now segment the CSI based on the birefringence of the sclera. The idea is as follows: we observe a certain, well defined retardation value δ_{pr} in the photoreceptor layer (averaged over the IS/OS and ETPR boundaries). The RPE and the choroid are non-birefringent, therefore the retardation value should stay constant within these layers. The retardation rises within the sclera, so we have to find the position where the retardation starts to increase; this position should correspond to the CSI. However, the depolarization of light backscattered from the RPE and parts of the choroid mimic an increased retardation of parts of the signal observed in these layers (cf. the retardation A-scan shown in Fig. 1(d), which shows noisy peaks in front of the sclera). Therefore, our segmentation algorithm starts searching a retardation gradient from the posterior side of the image, excluding areas of unreliable signal (the grey areas of Fig. 1(c)). Within the slope of the gradient (dashed red line), the depth position z_1 where the retardation drops below a predetermined value δ_1 is located. Ideally, δ_1 would be equal to δ_{pr}. However, because of the noisy retardation signal in the choroid, the

retardation does not drop to the value of δ_{pr}. Therefore, we add an offset to define δ_1: $\delta_1 = \delta_{pr} + \delta_{offset}$. The optimum choice of δ_{offset} was empirically found to be $\delta_{offset} = 14°$. The position z_1 of δ_1 is slightly deeper than the theoretic CSI position z_{CSI} (which is where the retardation value would have dropped to δ_{pr} if there were no disturbance by the noisy choroid signal). We approximate $z_{CSI} = z_1 - (dz/d\delta)\delta_{offset}$, where $(dz/d\delta)$ is the inverse gradient of the retardation (we take a mean retardation gradient (i.e., birefringence) of 0.62°/μm optical imaging depth for all subjects).

To reduce noise and improve segmentation results, the retardation image is median filtered before the algorithm to search z_{CSI} is applied. To remove outliers caused by noise, a polynomial of 4th order is fit to the raw z_{CSI} values. z_{CSI} values that deviate by more than 55 μm from the fitted line are removed and replaced by the polynomial values. Finally, the result is smoothed by a median filter. The resulting CSI is shown as a green and white line in Figs. 1(e) and (f), respectively. (Since the exact position of the CSI is still controversial if intensity and retardation data are compared (see discussion) we decided to refrain from further smoothing this line by fitting to a polynomial; therefore, it has a rather wavy appearance which, however, allows a more detailed comparison with small-scale structures observed in the intensity images.)

3. Results

Horizontal cross sections of the fovea region of the right eye of five healthy subjects were recorded, and RPE and CSI were segmented as described above. Figure 2 shows the results. Left and right hand columns show intensity and retardation images, respectively. RPE and CSI segmentation lines are shown in red and green in the intensity images, respectively, and as two white lines in the retardation images.

Figure 3 shows a plot of the choroidal thickness (CT) extracted from these images. CT was calculated as the difference between the CSI and RPE line, divided by an estimated refractive index of 1.4. CT varies among subjects, with mean CT values ranging from 271 to 383 μm (averaged over the width of the individual B-scans). The CT within a B-scan is not uniform but can show a strong asymmetry, e.g., in Fig. 2(a) and 2(b) the maximum value is 343 μm (slightly temporal to the foveola), while the minimum value is 205 μm (at the nasal edge of the imaged region).

Figure 4 shows results of a repeatability measurement (same eye as in Fig. 2(a) and 2(b)). The eye was repeatedly measured 5 times. The mean CT line and the interval of the standard deviation (SD) are shown. The mean SD (across the width of the B-scan) was 17.5 μm. The mean SD value of all 5 eyes was 18.3 μm (range: 13 – 28 μm).

4. Discussion

We developed and demonstrated a new method to measure choroidal thickness by PS-OCT, based entirely on polarization sensitive, intrinsic, tissue specific contrast mechanisms. While the anterior boundary of the choroid, the RPE, was segmented based on depolarization, the segmentation of the posterior boundary, the CSI, is based on the birefringence of the sclera.

While RPE segmentation by PS-OCT has been reported previously for OCT at 840 nm wavelength [35], we show here for the first time that it works equally well at 1040 nm. To smoothen the RPE contour, a polynomial of 4th order was fitted to the data found by the polarization-based algorithm. One might argue that this method to segment the anterior choroidal boundary might not work in patients with a distorted RPE, e.g., in case of diseases affecting the RPE, like drusen or geographic atrophy in age related macular degeneration, where the RPE is distorted or totally missing. However, we have developed more sophisticated algorithms based on iterative contour fitting that reliably identify the anterior choroidal boundary even in these conditions [36].

The segmentation of the CSI by exploiting the scleral birefringence is somewhat more complicated, for two reasons:

(i) The penetration depth of 840 nm OCT systems is usually not good enough to image the CSI. The reasons are the increased scattering of the shorter wavelength in RPE and choroid, and the stronger sensitivity roll off of usual spectrometer based 840 nm SD-OCT systems. The use of the less scattered longer wavelength of ~1050 nm, emitted by a swept source with low sensitivity roll off, improved the penetration depth considerably, enabling reliable identification of the CSI in most cases. (It should, however, be mentioned that intensity based imaging of the CSI by 840 nm OCT systems operated in reverse mode (“enhanced depth imaging”, or EDI mode), in combination with averaging supported by a retinal tracker, has recently been successfully demonstrated [18, 42, 43].)

(ii) Contrary to depolarization, which can easily be identified also in very thin layers like the mono-cell RPE layer, retardation caused by birefringence requires a certain layer thickness to build up a measurable retardation: a gradient has to be searched, and the position where this gradient starts has to be identified. The search for the gradient is complicated by two effects: the noisy retardation signal caused by the depolarizing pigments in the choroid, and the multiple scattering observed at very deep positions, which also leads to confounding noise of the measured retardation signal. Our solution to these problems was to gate out multiply scattered light via the DOPU value, and to start the search for the retardation gradient from the posterior side of the image. While this method worked well in the majority of the subjects imaged in this study, it can lead to limitations: In case of very thick choroids (CT > ~380 - 400 μm), the signal from the sclera might be dominated by multiply scattered light, preventing the measurement of reliable retardation signals from the sclera over a depth interval that is necessary to identify the retardation gradient. We observed such an effect in one of our subjects (cf. Figs. 2(g), 2(h)). In this case, most of the data points below the choroid are associated with low DOPU values, so the resulting segmentation line is questionable. This is in agreement with the fact that the repeatability of CT measurement was worst in this subject (SD = 28 μm).

The mean variability (SD) of 18.3 μm observed in our subjects corresponds to ~5 – 6% of the measured mean CT. This value is of the order of the diurnal variability of choroidal

thickness which has a mean amplitude of 33.7 μm [44]. However, it should be mentioned that locally higher values of variability are found (cf. Fig. 4, e.g. near the foveola and at ~2° nasal eccentricity). This locally increased variability is likely caused by slightly different fixation of the subject between different B-scan series. Local anatomic variations, e.g. near large vessels, can lead to CT values that slightly differ from one measurement to the next in these areas. A possible solution might be to obtain 3D data sets and derive 2D CT maps, whereby B-scan averaging over adjacent B-scans might be used. This would require a careful balance between the trade-offs between resolution in y-direction, sensitivity, and total measuring time.

In most previous studies, CSI segmentation and CT measurements were done manually on intensity images. To compare the CSI segmentation results obtained by our polarization based algorithm to manual, intensity based segmentation, we selected one data set obtained from each subject and manually drew a segmentation line into the intensity image.

Figure 5 shows an example of B-scans with segmentation lines for a detailed comparison (same subject as in Fig. 2 (c), 2(d)). Figure 5(a) shows the intensity image, Fig. 5(b) the retardation image. In addition to the PS-OCT based segmentation lines, the manually drawn lines are shown in orange (the line was drawn into the intensity image and copied into the retardation image). On the right hand side (nasal, area is close to the optic nerve head) the PS-OCT based CSI segmentation line is close to the manually drawn line. However, in other parts (left hand side), there is a distinct deviation: the PS-OCT segmentation line is placed deeper than the intensity based line. Part of that deviation might be caused by the fact that we used an average scleral birefringence to correct for the retardation offset δ_{offset} (cf. section 2.3). The retardation image clearly shows that the birefringence (color gradient) is not constant along the B-scan. An individually and locally varying birefringence could be implemented in future improvements of our algorithm. However, this effect can only explain a minor part of the observed deviation. The retardation image clearly shows that the PS-OCT line is at the position where the retardation gradient (i.e. the birefringence) starts, the intensity-based line is within an area that shows constant retardation (no birefringence).

A comparison of Figs. 5(a) and 5(b) clearly shows that in the corresponding areas there are quite thick regions within the tissue of rather uniform reflectivity that show no birefringence (constant blue color in Fig. 5(b), cf. asterisks). This leads to a unilateral deviation of PS-OCT and intensity based CSI segmentation. The PS algorithm tends to draw the segmentation line at a deeper position than intensity based manual segmentation. In Fig. 5, the deviation ranges from 0 to ~70 μm, with an average of ~25 μm. Across all five volunteers, the mean deviation is ~35 μm.

The reasons for these discrepancies are still under discussion: either the tissue layer where the discrepancy is observed is not part of the sclera or the corresponding scleral tissue is non-birefringent. Therefore, the true CSI position remains unclear in these areas, and further research and comparison with histology is needed.

Despite this unresolved discrepancy, we think CT segmentation by PS-OCT is an interesting alternative to intensity based methods because it can be fully automated and provides additional, complementary information to intensity based data.

(We would like to note that during the review process of our manuscript, an independent paper reporting a related algorithm to segment the CSI based on the scleral birefringence has been published [45].)

Acknowledgments

Financial support from the European Union (project FUN OCT, FP7 HEALTH, contract no. 201880) and from the Austrian Science Fund (FWF grant P19624-B02) is gratefully acknowledged.

References and Links

1. Huang D, Swanson EA, Lin CP, Schuman JS, Stinson WG, Chang W, Hee MR, Flotte T, Gregory K, Puliafito CA, Fujimoto JG. Optical coherence tomography. Science. 1991; 254(5035):1178–1181. [PubMed: 1957169]
2. Fercher AF, Drexler W, Hitzenberger CK, Lasser T. Optical coherence tomography - principles and applications. Rep. Prog. Phys. 2003; 66(2):239–303.
3. Drexler, W.; Fujimoto, JG. Optical coherence tomography. Technology and Applications. Springer; Berlin: 2008.
4. Drexler W, Fujimoto JG. Optical coherence tomography in ophthalmology. J. Biomed. Opt. 2007; 12(4):041201.
5. Geitzenauer W, Hitzenberger CK, Schmidt-Erfurth UM. Retinal optical coherence tomography: past, present and future perspectives. Br. J. Ophthalmol. 2011; 95(2):171–177. [PubMed: 20675732]
6. Fercher AF, Hitzenberger CK, Kamp G, Elzaiat SY. Measurement of intraocular distances by backscattering spectral interferometry. Opt. Commun. 1995; 117(1-2):43–48.
7. Häusler G, Lindner MW. “Coherence radar” and “spectral radar” - new tools for dermatological diagnosis. J. Biomed. Opt. 1998; 3(1):21–31. [PubMed: 23015002]
8. Wojtkowski M, Leitgeb R, Kowalczyk A, Bajraszewski T, Fercher AF. In vivo human retinal imaging by Fourier domain optical coherence tomography. J. Biomed. Opt. 2002; 7(3):457–463. [PubMed: 12175297]
9. Leitgeb R, Hitzenberger CK, Fercher AF. Performance of fourier domain vs. time domain optical coherence tomography. Opt. Express. 2003; 11(8):889–894. [PubMed: 19461802]
10. de Boer JF, Cense B, Park BH, Pierce MC, Tearney GJ, Bouma BE. Improved signal-to-noise ratio in spectral-domain compared with time-domain optical coherence tomography. Opt. Lett. 2003; 28(21):2067–2069. [PubMed: 14587817]
11. Choma MA, Sarunic MV, Yang CH, Izatt JA. Sensitivity advantage of swept source and Fourier domain optical coherence tomography. Opt. Express. 2003; 11(18):2183–2189. [PubMed: 19466106]
12. Unterhuber A, Povazay B, Hermann B, Sattmann H, Chavez-Pirson A, Drexler W. In vivo retinal optical coherence tomography at 1040 nm - enhanced penetration into the choroid. Opt. Express. 2005; 13(9):3252–3258. [PubMed: 19495226]
13. Yasuno Y, Hong YJ, Makita S, Yamanari M, Akiba M, Miura M, Yatagai T. In vivo high-contrast imaging of deep posterior eye by 1-microm swept source optical coherence tomography and scattering optical coherence angiography. Opt. Express. 2007; 15(10):6121–6139. [PubMed: 19546917]
14. Lee ECW, de Boer JF, Mujat M, Lim H, Yun SH. In vivo optical frequency domain imaging of human retina and choroid. Opt. Express. 2006; 14(10):4403–4411. [PubMed: 19516592]

15. Puvanathasan P, Forbes P, Ren Z, Malchow D, Boyd S, Bizheva K. High-speed, high-resolution Fourier-domain optical coherence tomography system for retinal imaging in the 1060 nm wavelength region. Opt. Lett. 2008; 33(21):2479–2481. [PubMed: 18978893]
16. Esmaeelpour M, Povazay B, Hermann B, Hofer B, Kajic V, Kapoor K, Sheen NJL, North RV, Drexler W. Three-dimensional 1060-nm OCT: choroidal thickness maps in normal subjects and improved posterior segment visualization in cataract patients. Invest. Ophthalmol. Vis. Sci. 2010; 51(10):5260–5266. [PubMed: 20445110]
17. Esmaeelpour M, Považay B, Hermann B, Hofer B, Kajic V, Hale SL, North RV, Drexler W, Sheen NJL. Mapping choroidal and retinal thickness variation in type 2 diabetes using three-dimensional 1060-nm optical coherence tomography. Invest. Ophthalmol. Vis. Sci. 2011; 52(8):5311–5316. [PubMed: 21508108]
18. Ikuno Y, Maruko I, Yasuno Y, Miura M, Sekiryu T, Nishida K, Iida T. Reproducibility of retinal and choroidal thickness measurements in enhanced depth imaging and high-penetration optical coherence tomography. Invest. Ophthalmol. Vis. Sci. 2011; 52(8):5536–5540. [PubMed: 21508114]
19. Kajić V, Esmaeelpour M, Považay B, Marshall D, Rosin PL, Drexler W. Automated choroidal segmentation of 1060 nm OCT in healthy and pathologic eyes using a statistical model. Biomed. Opt. Express. 2012; 3(1):86–103. [PubMed: 22254171]
20. Hee MR, Huang D, Swanson EA, Fujimoto JG. Polarization-sensitive low-coherence reflectometer for birefringence characterization and ranging. J. Opt. Soc. Am. B. 1992; 9(6):903–908.
21. de Boer JF, Milner TE, van Gemert MJC, Nelson JS. Two-dimensional birefringence imaging in biological tissue by polarization-sensitive optical coherence tomography. Opt. Lett. 1997; 22(12): 934–936. [PubMed: 18185711]
22. Weinreb RN, Dreher AW, Coleman A, Quigley H, Shaw B, Reiter K. Histopathologic validation of Fourier-ellipsometry measurements of retinal nerve fiber layer thickness. Arch. Ophthalmol. 1990; 108(4):557–560. [PubMed: 2322159]
23. Cense B, Chen TC, Park BH, Pierce MC, de Boer JF. In vivo depth-resolved birefringence measurements of the human retinal nerve fiber layer by polarization-sensitive optical coherence tomography. Opt. Lett. 2002; 27(18):1610–1612. [PubMed: 18026517]
24. Brink HB, van Blokland GJ. Birefringence of the human foveal area assessed in vivo with Mueller-matrix ellipsometry. J. Opt. Soc. Am. A. 1988; 5(1):49–57. [PubMed: 3351653]
25. Pircher M, Götzinger E, Leitgeb R, Sattmann H, Findl O, Hitzenberger CK. Imaging of polarization properties of human retina in vivo with phase resolved transversal PS-OCT. Opt. Express. 2004; 12(24):5940–5951. [PubMed: 19488235]
26. Baumann B, Götzinger E, Pircher M, Hitzenberger CK. Single camera based spectral domain polarization sensitive optical coherence tomography. Opt. Express. 2007; 15(3):1054–1063. [PubMed: 19532333]
27. Yamanari M, Makita S, Yasuno Y. Polarization-sensitive swept-source optical coherence tomography with continuous source polarization modulation. Opt. Express. 2008; 16(8):5892–5906. [PubMed: 18542701]
28. Michels S, Pircher M, Geitzenauer W, Simader C, Götzinger E, Findl O, Schmidt-Erfurth U, Hitzenberger CK. Value of polarisation-sensitive optical coherence tomography in diseases affecting the retinal pigment epithelium. Br. J. Ophthalmol. 2008; 92(2):204–209. [PubMed: 18227201]
29. Cense B, Chen TC, Park BH, Pierce MC, de Boer JF. Thickness and birefringence of healthy retinal nerve fiber layer tissue measured with polarization-sensitive optical coherence tomography. Invest. Ophthalmol. Vis. Sci. 2004; 45(8):2606–2612. [PubMed: 15277483]
30. Mujat M, Park BH, Cense B, Chen TC, de Boer JF. Autocalibration of spectral-domain optical coherence tomography spectrometers for in vivo quantitative retinal nerve fiber layer birefringence determination. J. Biomed. Opt. 2007; 12(4):041205. [PubMed: 17867794]
31. Yamanari M, Miura M, Makita S, Yatagai T, Yasuno Y. Phase retardation measurement of retinal nerve fiber layer by polarization-sensitive spectral-domain optical coherence tomography and scanning laser polarimetry. J. Biomed. Opt. 2008; 13(1):014013. [PubMed: 18315371]

32. Götzinger E, Pircher M, Baumann B, Hirn C, Vass C, Hitzenberger CK. Retinal nerve fiber layer birefringence evaluated with polarization sensitive spectral domain OCT and scanning laser polarimetry: A comparison. J Biophoton. 2008; 1(2):129–139.
33. Pircher M, Götzinger E, Findl O, Michels S, Geitzenauer W, Leydolt C, Schmidt-Erfurth U, Hitzenberger CK. Human macula investigated in vivo with polarization-sensitive optical coherence tomography. Invest. Ophthalmol. Vis. Sci. 2006; 47(12):5487–5494. [PubMed: 17122140]
34. Götzinger E, Pircher M, Baumann B, Ahlers C, Geitzenauer W, Schmidt-Erfurth U, Hitzenberger CK. Three-dimensional polarization sensitive OCT imaging and interactive display of the human retina. Opt. Express. 2009; 17(5):4151–4165. [PubMed: 19259252]
35. Götzinger E, Pircher M, Geitzenauer W, Ahlers C, Baumann B, Michels S, Schmidt-Erfurth U, Hitzenberger CK. Retinal pigment epithelium segmentation by polarization sensitive optical coherence tomography. Opt. Express. 2008; 16(21):16410–16422. [PubMed: 18852747]
36. Baumann B, Götzinger E, Pircher M, Sattmann H, Schuutze C, Schlanitz F, Ahlers C, Schmidt-Erfurth U, Hitzenberger CK. Segmentation and quantification of retinal lesions in age-related macular degeneration using polarization-sensitive optical coherence tomography. J. Biomed. Opt. 2010; 15(6):061704. [PubMed: 21198152]
37. Ahlers C, Götzinger E, Pircher M, Golbaz I, Prager F, Schütze C, Baumann B, Hitzenberger CK, Schmidt-Erfurth U. Imaging of the retinal pigment epithelium in age-related macular degeneration using polarization-sensitive optical coherence tomography. Invest. Ophthalmol. Vis. Sci. 2010; 51(4):2149–2157. [PubMed: 19797228]
38. Götzinger E, Pircher M, Hitzenberger CK. High speed spectral domain polarization sensitive optical coherence tomography of the human retina. Opt. Express. 2005; 13(25):10217–10229. [PubMed: 19503236]
39. Hitzenberger CK, Goetzinger E, Sticker M, Pircher M, Fercher AF. Measurement and imaging of birefringence and optic axis orientation by phase resolved polarization sensitive optical coherence tomography. Opt. Express. 2001; 9(13):780–790. [PubMed: 19424315]
40. Götzinger E, Pircher M, Baumann B, Schmoll T, Sattmann H, Leitgeb RA, Hitzenberger CK. Speckle noise reduction in high speed polarization sensitive spectral domain optical coherence tomography. Opt. Express. 2011; 19(15):14568–14585. [PubMed: 21934820]
41. Schoenenberger K, Colston BW, Maitland DJ, Da Silva LB, Everett MJ. Mapping of birefringence and thermal damage in tissue by use of polarization-sensitive optical coherence tomography. Appl. Opt. 1998; 37(25):6026–6036. [PubMed: 18286100]
42. Spaide RF, Koizumi H, Pozzoni MC. Enhanced depth imaging spectral-domain optical coherence tomography. Am. J. Ophthalmol. 2008; 146(4):496–500. [PubMed: 18639219]
43. Rahman W, Chen FK, Yeoh J, Patel P, Tufail A, Da Cruz L. Repeatability of manual subfoveal choroidal thickness measurements in healthy subjects using the technique of enhanced depth imaging optical coherence tomography. Invest. Ophthalmol. Vis. Sci. 2011; 52(5):2267–2271. [PubMed: 21087970]
44. Tan CS, Ouyang Y, Ruiz H, Sadda SR. Diurnal variation of choroidal thickness in normal, healthy subjects measured by spectral domain optical coherence tomography. Invest. Ophthalmol. Vis. Sci. 2012; 53(1):261–266. [PubMed: 22167095]
45. Duan L, Yamanari M, Yasuno Y. Automated phase retardation oriented segmentation of chorio-scleral interface by polarization sensitive optical coherence tomography. Opt. Express. 2012; 20(3):3353–3366. [PubMed: 22330573]

Europe PMC Funders Author Manuscripts

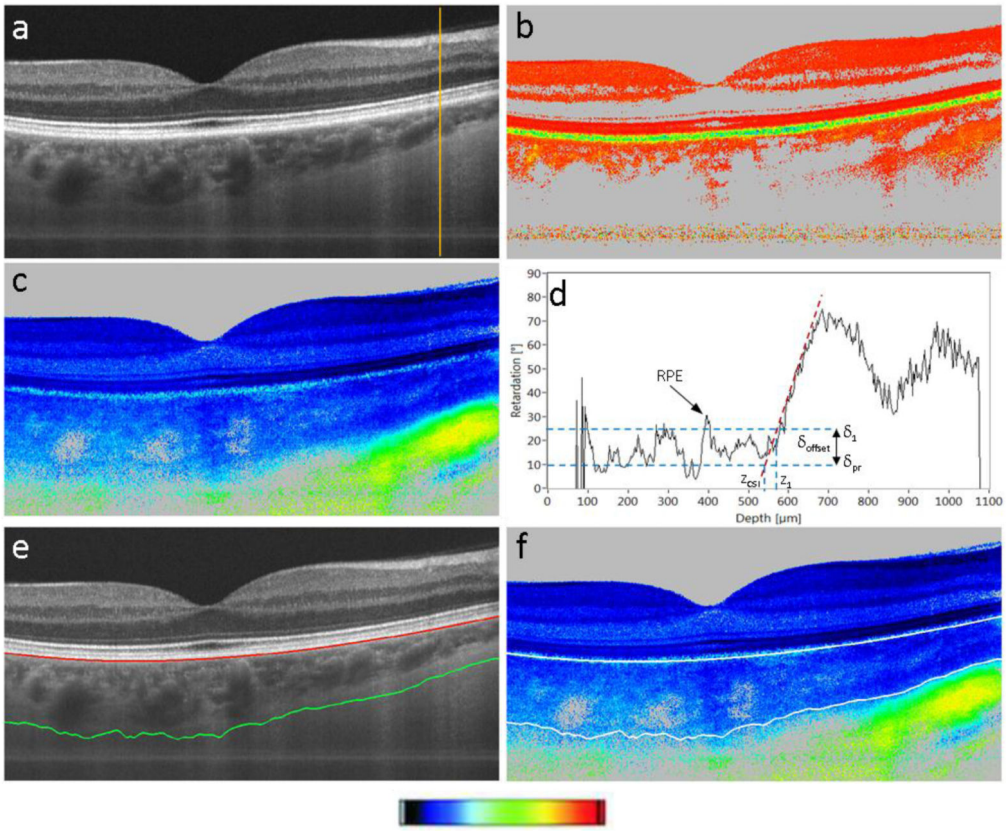

Fig. 1.

PS-OCT images of human fovea region to illustrate segmentation of choroid. a) Intensity B-scan; b) DOPU B-scan (color bar: 0-1); c) retardation B-scan (color bar: 0° - 90°); d) retardation A-scan (position shown by orange line in a)); e) intensity B-scan with segmentation lines (red: RPE, green: CSI); f) retardation B-scan with segmentation lines (top white line: RPE, bottom white line: CSI, color bar: 0° - 90°). B-scan dimensions: 19° (horizontal) × 1 mm (vertical; geometric distance).

Europe PMC Funders Author Manuscripts

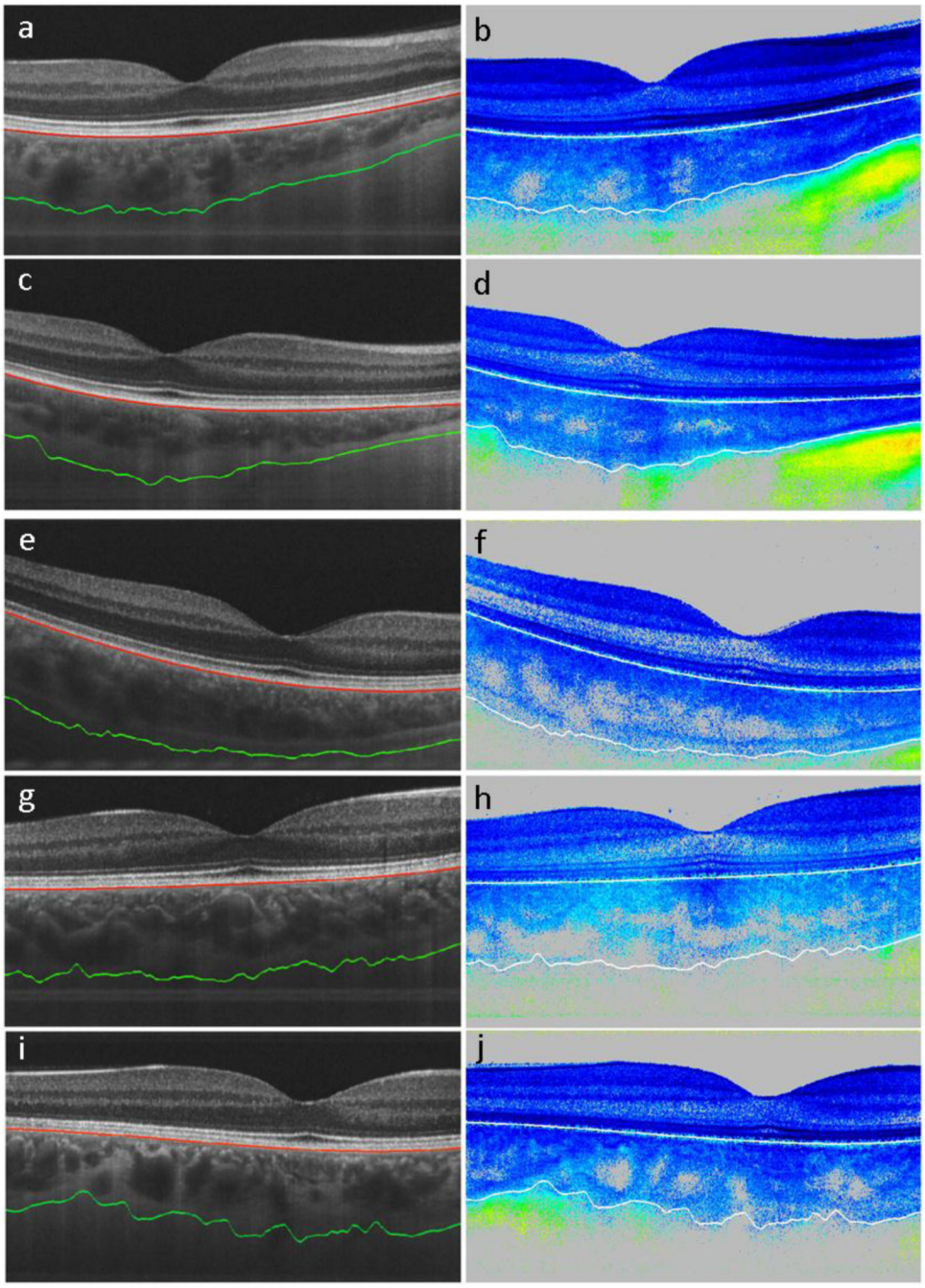

Fig. 2.

Segmentation of choroid in five healthy volunteers by PS-OCT. Left column: intensity B-scans (red line: RPE, green line: CSI). Right column: retardation B-scans (top white line: RPE, bottom white line: CSI; color scale: cf. Figure 1). B-scan dimensions: 19° (horizontal) × 1060 μm (vertical; geometric distance).

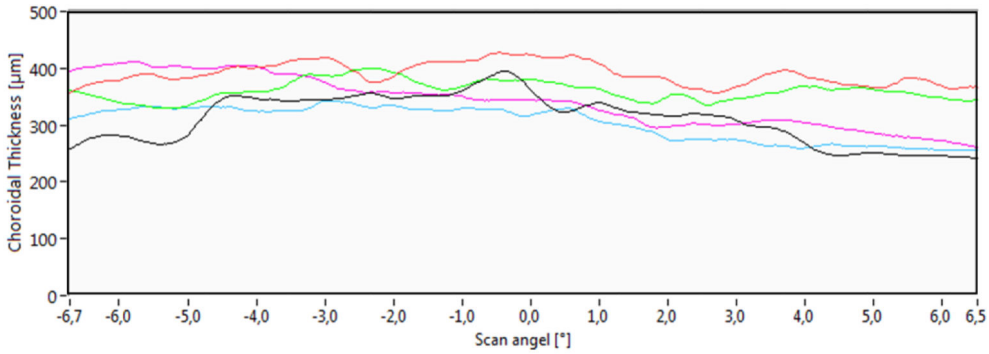

Fig. 3.

Plots of choroidal thickness obtained by PS-OCT in five healthy volunteers. The foveola is at 0° (left and right sides are cropped to cover only those parts of the horizontal scans that are imaged in all eyes; the cropping was necessary because of decentration of some scans, cf. Figure 2).

Europe PMC Funders Author Manuscripts

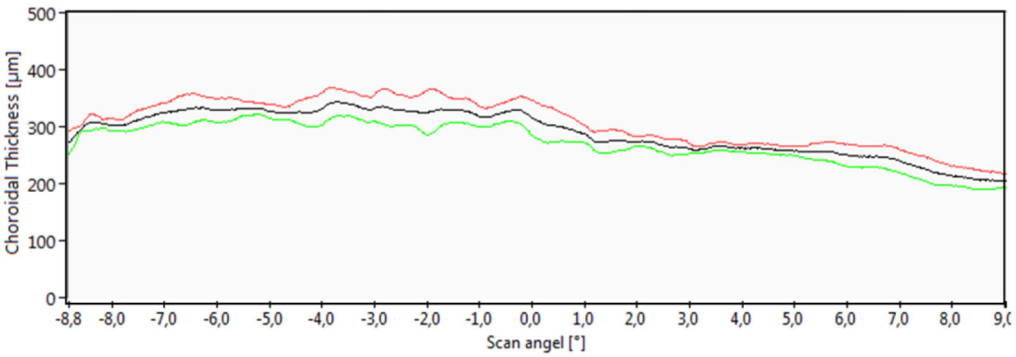

Fig. 4.

Repeatability of CT segmentation by PS-OCT. The center line (black) shows the mean value of 5 CT thickness measurements obtained in a single subject. The other lines (red and green) show mean ± standard deviation. The foveola is at 0°.

Europe PMC Funders Author Manuscripts

Europe PMC Funders Author Manuscripts

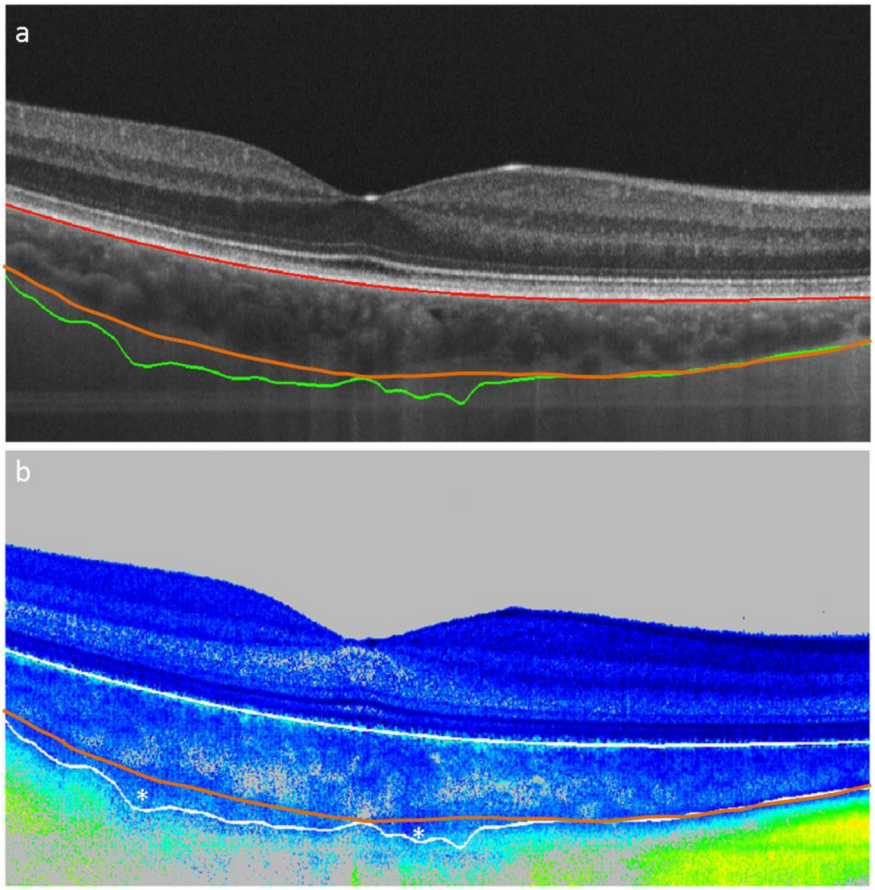

Fig. 5.

PS-OCT B-scans of a human retina to illustrate deviations between PS-OCT based choroidal segmentation and results derived manually from intensity image. See text for details. a) Intensity (red line: RPE, green line: CSI by PS-OCT, orange line: CSI by manual segmentation); b) retardation (top white line: RPE, bottom white line: CSI by PS-OCT, orange line: CSI by manual segmentation; color bar: cf. Fig. 1). B-scan dimensions: 19° (horizontal) × 1060 μm (vertical; geometric distance).